Orbital physics in sulfur spinels: ordered, liquid and glassy ground states

New Journal of Physics
The open–access journal for physics

Orbital physics in sulfur spinels: ordered, liquid and glassy ground states

N Büttgen[1], J Hemberger[1], V Fritsch[1], A Krimmel[1], M Mücksch[1], H-A Krug von Nidda[1], P Lunkenheimer[1], R Fichtl[1], V Tsurkan[1,2] and A Loidl[1]

[1] Experimental Physics V, Center for Electronic Correlations and Magnetism, Institute of Physics, University of Augsburg, D-86135 Augsburg, Germany
[2] Institute of Applied Physics, Academy of Science of Moldova, MD 2028 Chisinau, Republic of Moldova
E-mail: norbert.buettgen@physik.uni-augsburg.de

New Journal of Physics **6** (2004) 191
Received 19 July 2004
Published 7 December 2004
Online at http://www.njp.org/
doi:10.1088/1367-2630/6/1/191

Abstract. Measurements of magnetization $M(T, H)$, heat capacity $C(T)$, NMR lineshift $K(T)$ and linewidth $\Delta(T)$, neutron scattering $S(Q, \omega, T)$ and broadband dielectric spectroscopy $\epsilon(\omega, T)$ provide experimental evidence of the different orbital ground states in the cubic sulfur spinels under investigation. In all compounds, the tetrahedrally coordinated Jahn–Teller ions Fe^{2+} are characterized by a degeneracy of the orbital degrees of freedom. Particularly, we found a long-range orbital ordering in polycrystalline (PC) $FeCr_2S_4$, and a glassy freezing of the orbital degrees of freedom in $FeCr_2S_4$ (single crystals) (SCs). In contrast, $FeSc_2S_4$ belongs to the rare class of spin–orbital liquids, where quantum fluctuations accompanying the glassy freezing of the orbitals suppress long-range magnetic order.

PII: S1367-2630(04)83610-3

Contents

1. Introduction

Orbital physics has become a fascinating and important topic in modern solid-state physics and material science. In transition-metal oxides, the shape and anisotropy of the electron density of the d-derived electrons determine the fundamental electronic properties. The sensitivity of the magnetic exchange to the spatial orientation of the orbitals governs the long-range order of the spin degrees of freedom. If the orientational order of the orbitals can be changed by an external field (strain or electric field), the magnetic order will be changed concomitantly. The possibility to tune electronic orbitals by external fields has been recently proposed as an important ingredient of a future correlated electron technology [1]. From a more fundamental aspect, the strong coupling of spin, charge and orbital degrees of freedom yields complex and fascinating ground states. Usually, electron–phonon coupling lifts the orbital degeneracy and results in long-range orbital order (OO) and in a change of the crystal symmetry via the Jahn–Teller (JT) effect [2]. As has been pointed out by Kugel and Khomskii (KK) [3], in Mott–Hubbard insulators OO can also be established, if the orbital degeneracy is lifted via a purely electronic interaction. In these cases of dominating JT or KK-type interactions an orbitally ordered and structurally distorted ground state is expected.

Long-range OO can be suppressed by frustration effects. Frustration characterizes the inability of a system to establish a long-range-ordered ground state, despite strong interactions. So far, frustration effects have been extensively studied for the spin degrees of freedom. Frustration and disorder provide the key concept to understand the spin-glass state in disordered magnets [4]. But frustration can also govern fully ordered arrays of spins. A standard example for geometrical frustration is a triangular Ising-spin system with antiferromagnetic exchange. In these geometrically frustrated magnets, unusual ground states can evolve [5], which are characterized, e.g., by resonating valence bonds, or reveal spin order determined by Pauling's ice rules [6, 7] or a low-temperature spin-liquid state [8].

Recently, it has been suggested that exchange interactions between orbital degrees of freedom can be as strongly frustrated like spins and even in cubic lattices the orbitals may remain disordered down to 0 K, forming an orbital liquid (OL) [9]–[11]. Indeed, an OL state has been proposed for $LaTiO_3$ [12, 13] but has been questioned recently [14, 15]. To find new OL it

seems promising to search for systems with strong correlation effects and weak JT coupling. The appropriate candidates are Mott–Hubbard insulators with electrons with three-fold degeneracy in octahedral or two-fold degeneracy in tetrahedral crystal fields [11]. In addition, geometrical frustration effects in the orbital sector may enhance the tendency to form disordered spin ground states. Frustration results in a dynamic liquid ground state or in a glassy freezing of the internal degrees of freedom at low temperatures.

Spinel compounds are archetypical examples of geometrically frustrated systems. Already in 1956, Anderson [16] pointed out that the octahedral sites in the spinel structure form a frustrated lattice in which it is possible to achieve perfect short-range order while maintaining a finite entropy. Recently, we have demonstrated that the tetrahedral site of the normal spinel structure is also strongly frustrated, in the spin [17] as well as in the orbital sector [17, 18]. In this communication, we present structural, magnetic, heat capacity, nuclear magnetic resonance (NMR), neutron scattering, and dielectric-spectroscopy results of normal cubic spinels, where the A-site of the spinel structure carries the spin or orbital moment of interest. $FeCr_2S_4$ is a ferrimagnet with fully developed long-range magnetic order of the iron and chromium spins below 167 K. The Fe^{2+} ions, with a spin moment of $S = 2$, are located exclusively in the tetrahedral A-sites of the spinel structure and are JT active. Hence, long-range orbital order is expected at low temperatures. We demonstrate that the orbital moments are frustrated and the ground state is an orbital glass. In $FeSc_2S_4$, the B-site is non-magnetic and spin and orbital moments reside on the A-site, both being geometrically frustrated. The ground state in this compound turns out to be a spin liquid and an orbital glass. The orbital freezing is monitored by utilizing broadband dielectric techniques. The spin and orbital excitation spectrum is studied by neutron scattering techniques. The results on $FeSc_2S_4$ are compared to those obtained from $MnSc_2S_4$ with $S = 5/2$ and a half-filled d-shell which is JT inactive. In this case we find moderate spin frustration.

2. Experimental results and discussion

$FeCr_2S_4$, $FeSc_2S_4$ and $MnSc_2S_4$ crystallize in the normal cubic spinel structure ($Fd\bar{3}m$). In this normal AB_2X_4 spinel, the X-site anions build a close-packed face-centred cubic (fcc) lattice, where the A-site cations occupy 1/8 of the tetrahedrally coordinated interstices and the B-site anions occupy 1/2 of the octahedrally coordinated interstices. Concerning $FeCr_2S_4$, the Cr^{3+} sublattice, with an electronic configuration of $3d^3$ and $S = 3/2$, is octahedrally coordinated by the sulfur ions and is dominated by ferromagnetic exchange of the 90° Cr–S–Cr bond angle. In the octahedral crystal field, the 3d multiplet splits into a low-lying t_{2g} triplet with each of the three orbitals occupied by one electron with parallel spin, and by an unoccupied e_g-doublet. For the A-site, the Fe^{2+} ion is in a tetrahedral crystal field and the splitting is reversed with a lower e doublet and an upper t_2 triplet. Accordingly, the $3d^6$ electrons are Hund's rule coupled revealing a high-spin configuration with $S = 2$. The A-site ions are only weakly antiferromagnetically coupled within the sublattice, but much stronger to the B-site chromium ions and ferrimagnetic order is established below $T_C = 167$ K with the Fe^{2+} and Cr^{3+} magnetic moments aligned antiparallel to each other. In $FeSc_2S_4$ and $MnSc_2S_4$, the B-site is occupied by a non-magnetic ion. As outlined above, the d-orbital states of the tetrahedrally coordinated A-site ions reveal a lower doublet and an excited triplet of the d-electron manifold. The Mn^{2+} ion reveals a half-filled d-shell with a spin value $S = 5/2$ and zero orbital moment. The Fe^{2+} ion with $S = 2$ exhibits a hole in the lower doublet and, hence, is JT active. The A-site ions in the normal spinel form a diamond lattice,

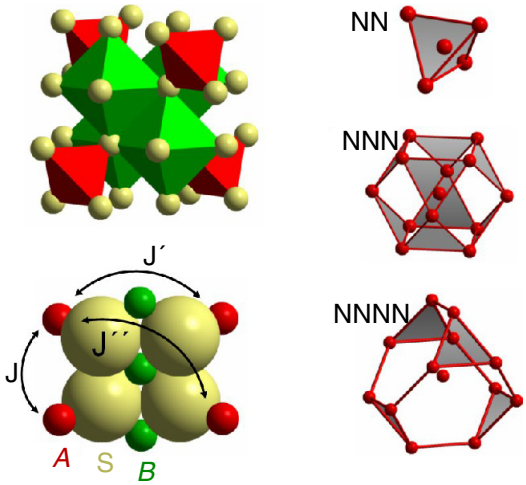

Figure 1. The structure of the AB_2S_4 spinel. The A-sites (red) are embedded in a tetrahedral environment of sulfur (yellow), while the B-sites (green) have octahedral environment (see upper left illustration). The A-site is mediated via three different types of A–S–B–S–A interaction paths. A plaquette containing nearest neighbours (NN), next-nearest neighbours (NNN) and next-next-nearest neighbours (NNNN) of the A-site lattice with exchange paths J, J' and J'', respectively, is displayed in the lower left illustration. J as well as J' triple exchange path contains an S–B–S bond angle close to 90° in contrast to the J'' exchange path with a 180° bond. Also the interaction paths have a different multiplicity: there are four NN with a 6-fold interaction path and 12 NNN with a 2-fold interaction path, resulting in a multiplicity for J and J' of 24 each. The interaction paths J'' to the 12 NNNN are only 1-fold. The right hand side shows the NN, NNN and NNNN shells of the A-site lattice. The dominating structure element of all three polyhedrons is the triangle. Especially, the triangles and hexagons of the NNNN shell reminds one of the Kagomé lattice, which is a paradigm of a frustrated lattice.

i.e., two fcc lattices at $(0, 0, 0)$ and $(1/4, 1/4, 1/4)$. The magnetic superexchange interactions between the A-ions are weakly antiferromagnetic and the corresponding exchange paths involve at least five ions [19]. An illustration of the A-site and its exchange paths is given in figure 1. Considering the entire lattice, the exchange between the two A-site sublattices is transferred as follows: the four nearest neighbours (NN) are connected via six A–X–B–X–A exchange paths including nearly rectangular X–B–X bonds. The 12 next-nearest neighbours (NNN) are connected via two equivalent A–X–B–X–A exchange paths, including again nearly rectangular X–B–X bonds of non-magnetic ions. The 12 next-next-nearest neighbours (NNNN) are coupled via one A–X–B–X–A exchange path, including a 180° X–B–X bond. Note that the NNN in the entire lattice corresponds to the nearest neighbours within each fcc sublattice. We conclude that each fcc sublattice is coupled antiferromagnetically and, hence, is frustrated. In addition, the two sublattices are coupled again antiferromagnetically, strongly enforcing the frustration effects.

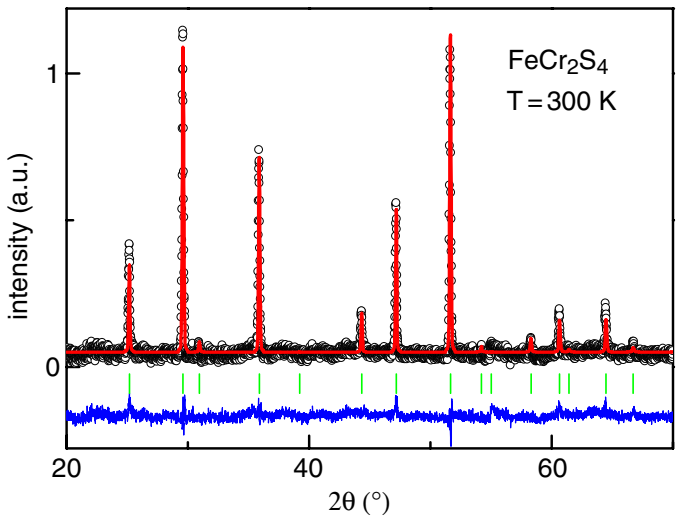

Figure 2. Diffraction pattern of $FeCr_2S_4$ at $T = 300$ K. The solid lines represent fits of a Rietveld analysis. The difference spectra shown below the data demonstrate the absence of any impurity phases.

2.1. Structural details

$FeCr_2S_4$ polycrystals (PCs) were prepared by solid-state reaction from the high-purity elements. The single crystals (SCs) were grown by a chemical-transport-reaction method with chlorine as transport agent. $FeSc_2S_4$ and $MnSc_2S_4$ have been prepared by solid-state reaction in PC form. Details of the synthesis and sample preparation have been described previously [17, 18]. The samples were investigated by standard x-ray techniques using Cu K_α radiation. A representative room-temperature spectrum of $FeCr_2S_4$ is shown in figure 2. From a detailed Rietveld refinement (solid line in figure 2) the lattice constant a and the fractional coordinate x of the sulfur atom were determined. Results for all the samples are summarized in table 1. The deviation of the sulfur parameter x from the ideal value $1/4$ indicates a slight trigonal distortion of the octahedra around the B-sites, while the tetrahedra remain undistorted. In $Fe/MnSc_2S_4$, this slight trigonal distortion yields X–B–X bonds of 92.3° for the Fe compound and 93.6° for the Mn compound in good agreement with [20]. To search for structural phase transitions in the JT active compound $FeSc_2S_4$, we performed a diffraction analysis down to 1.6 K (see section 2.5). We found no indications of a structural distortion and even the positions of the sulfur atoms within the unit cell remained constant within experimental uncertainties. As we will describe in detail below, heat capacity and dielectric experiments in $FeCr_2S_4$ reveal different low-temperature properties for SCs compared to PCs. For this reason the stoichiometric composition was carefully investigated by inductive-coupled plasma as well as micro probe analysis. Both modifications exhibited a nearly perfect Fe : Cr ratio, only the sulfur content of the SC was disturbed by about 1% chlorine out of the transport agent. This leads to free charge carriers which can suppress a cooperative JT effect resembling to oxygen excess in $LaMnO_3$ [21].

2.2. Magnetic properties

The magnetization measurements were performed with a commercial SQUID magnetometer for temperatures $1.7 \leqslant T \leqslant 400$ K and in applied fields up to 50 kOe. In order to obtain the

Table 1. Parameters from x-ray investigations.

	Lattice constant a (Å)	Fractional coordinate x
$FeCr_2S_4$	9.997 ± 0.001	0.259 ± 0.001
$FeSc_2S_4$	10.519 ± 0.007	0.255 ± 0.001
$MnSc_2S_4$	10.621 ± 0.007	0.257 ± 0.001

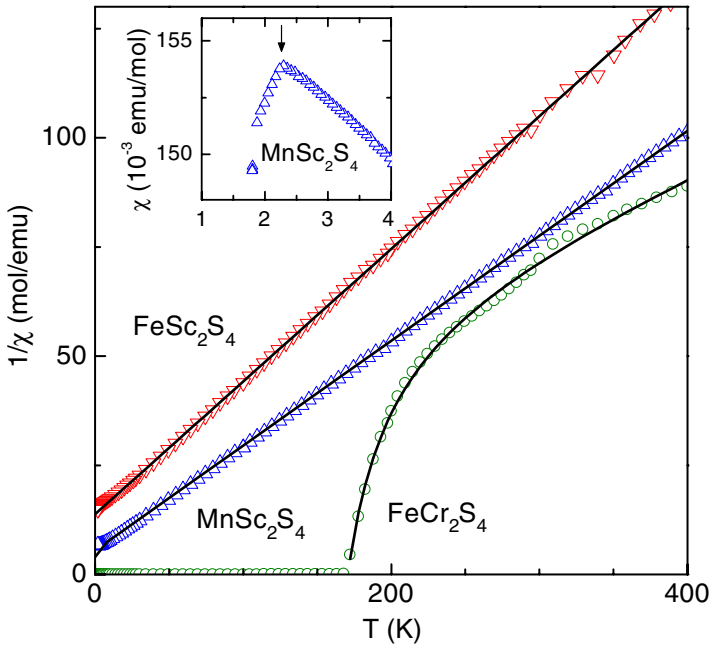

Figure 3. Inverse susceptibility $1/\chi(T)$ of $FeSc_2S_4$ (red triangles down), $MnSc_2S_4$ (blue triangles up) and $FeCr_2S_4$ (green circles), respectively. The susceptibility $\chi(T)$ is given by the ratio $M(T)/H$ (see text). The straight solid lines are linear fits with a CW law $\chi = C/(T - \Theta_{CW})$. The inverse susceptibility of $FeCr_2S_4$ has been fitted with the two-sublattice model for a ferrimagnet according to Goodenough [22]. Inset: susceptibility $\chi(T)$ versus T at low temperatures of $MnSc_2S_4$. The arrow indicates the transition into long-range magnetic ordering.

temperature-dependent susceptibility $\chi(T)$, we divided the magnetization $M(T)$ by the applied magnetic field H. The values of the applied magnetic field were $H = 1000$ Oe in the case of $Fe/MnSc_2S_4$ and 100 Oe in the case of $FeCr_2S_4$, respectively. Figure 3 shows the inverse susceptibilities $1/\chi(T)$ of $FeCr_2S_4$ (circles), $MnSc_2S_4$ (triangles up) and $FeSc_2S_4$ (triangles down) for $1.7 \leqslant T \leqslant 400$ K. To determine the paramagnetic moments $\mu_{eff} = p \cdot \mu_B$ and Curie–Weiss (CW) temperatures Θ_{CW}, we took the average of a series of measurements of different batches, where we used as grown samples and samples tempered in vacuum as well as in sulfur atmosphere. Despite these different treatments, we observed marginal changes of p and Θ_{CW} only, which are included in the error bars given in table 2. In the case of the compounds with non-magnetic B-sites ($Fe/MnSc_2S_4$), we observed perfect CW laws. In the case of $FeCr_2S_4$, the inverse paramagnetic susceptibility exhibits a concave curvature approaching the magnetic transition temperature as typical for ferrimagnets (see figure 3). We tried to fit these data employing a

Table 2. Parameters from magnetization measurements: measured effective Bohr magneton number p, CW temperature Θ_{CW} and transition temperature T_m. Additionally, the theoretically expected spin-only values are given.

	p	$2\sqrt{S(S+1)}$	Θ_{CW} (K)	T_m (K)
$FeCr_2S_4$	7.16 ± 0.3	7.35	-216 ± 40	$T_c = 167$
$FeSc_2S_4$	5.12 ± 0.1	4.9	-45.1 ± 1	–
$MnSc_2S_4$	5.77 ± 0.12	5.92	-22.9 ± 0.8	$T_N = 2.2$

CW-type approach considering two interacting magnetic sublattices [22]. The evaluated paramagnetic moments of $\mu_{eff} = p \cdot \mu_B$ were determined as summarized in table 2. However, for $FeCr_2S_4$ a noticeable uncertainty has to be considered due to the limited evaluable temperature regime. Within this error bar the value of the total effective Bohr magneton number p is in accordance with the expected spin-only value for one Fe^{2+} ($3d^6$, high spin) and two Cr^{3+} ($3d^3$) ions per formula unit of $p = 7.35$. The most significant deviation between the experimentally determined and the spin-only value of the effective Bohr magneton number p occurs for $FeSc_2S_4$. Here, the expected spin-only value of $p = 4.90$ is clearly below the experimental value (see table 2). The enhanced value of the experiment signals the influence of spin–orbit coupling, resulting in an effective g-value of 2.09, typically observed in iron compounds with Fe^{2+}.

The Cr compound exhibits a magnetic transition into a long-range-ordered spin state at $T_c = 167$ K. The negative CW temperature of $\Theta_{CW} \approx -200$ K, evaluated from the paramagnetic high-temperature regime, additionally corroborates the ferrimagnetic spin arrangement. In contrast, the Sc compounds do not show any sign of long-range order down to 2.2 K in the case of $MnSc_2S_4$ (see inset of figure 3) and even down to the lowest measured temperatures in the case of $FeSc_2S_4$. Nevertheless, one finds finite CW temperatures of $\Theta_{CW} = (-45.1 \pm 1)$ K for the iron and $\Theta_{CW} = (-22.9 \pm 0.8)$ K for the manganese compound, respectively. This denotes a very high degree of frustration, which can be described by the ratio $f = -\Theta_{CW}/T_N = 11.5$ ($MnSc_2S_4$) or even $f > 900$ ($FeSc_2S_4$) [17]. The latter value is one of the largest documented in literature. The upper frame of figure 4 displays the magnetic field dependence of the magnetization $M(H)$ in highly frustrated $FeSc_2S_4$ at 1.8 and 40 K. The solid lines are fits using a Brillouin function with an effective mean-field interaction. The corresponding fitting parameter resembles the CW temperature of $\Theta_{CW} = -45$ K as obtained from the inverse susceptibility data. The deviations from linear behaviour are monitored via the $M/H(H)$ representation in the lower frame of figure 4. Only at lowest temperatures a small decrease of $M/H(H)$ towards higher applied fields can be detected, which, however, could be explained by the presence of impurity spins (<0.5%) being saturated in the applied field. But no indication of any saturation effects is observed for the intrinsic Fe^{2+} spin system. Again, this type of behaviour underlines the presence of strong antiferromagnetic spin interactions, which are clearly dominating the applied fields but do not lead to a long-range order because of frustration.

2.3. Heat capacity

The heat-capacity experiments were conducted in non-commercial setups using a quasi-adiabatic method for $2.5 < T < 30$ K and an ac technique for $15 < T < 200$ K in a ^{4}He-cryostat. Below 2.5 K, the heat capacity has been measured in a ^{3}He/^{4}He dilution refrigerator with a relaxational

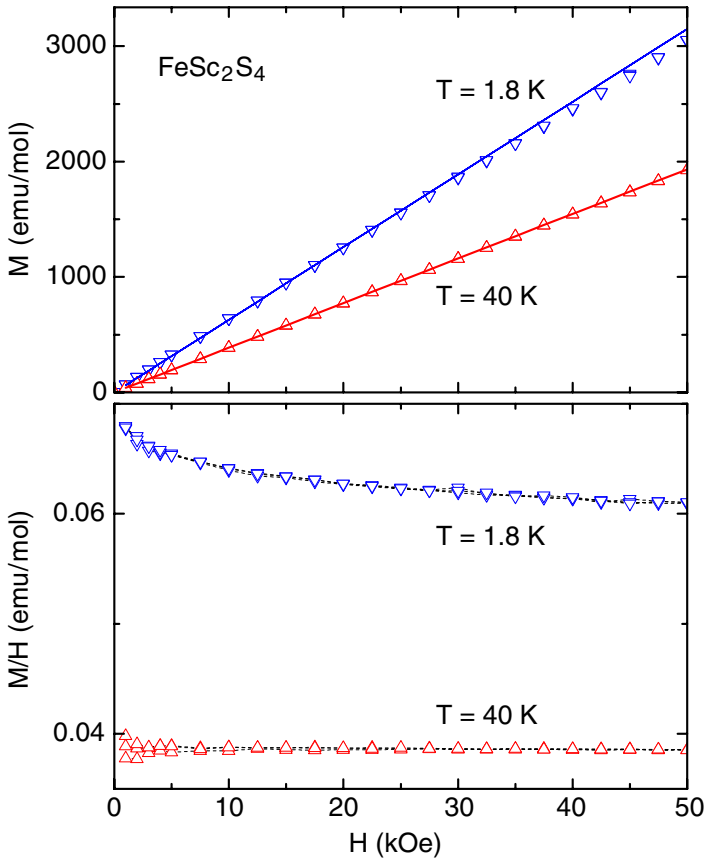

Figure 4. Upper panel: magnetization M versus applied magnetic field H of $FeSc_2S_4$. Lower panel: ratio M/H versus H of $FeSc_2S_4$. The solid lines are fits using a Brillouin function (see text).

method [17]. The upper frame of figure 5 shows the heat capacity of $FeCr_2S_4$ at low temperatures where C/T versus T is plotted. Results observed in the vacuum-annealed PC sample are compared to those for a SC. The PC reveals a well-defined OO transition at $T_{OO} = 10$ K, whereas in the SC this transition is completely suppressed. In the PC, the λ-type anomaly is followed by an exponential decrease of the heat capacity on decreasing temperature, indicative for the opening of a gap in the orbital excitations. This behaviour can be described within a BCS-like mean-field approach using a temperature-dependent gap energy $\Delta(T)$ approximated by $\Delta(T) \approx 1.74\Delta_0(1 - T/T_{OO})^{1/2}$. The best fit is obtained with the parameters $\Delta_0/k_B = 11.4$ K and $T_{OO} = 9.2$ K, yielding $2\Delta_0/k_B \approx 2.5T_{OO}$, which is strongly reduced as compared to the BCS value. The heat capacity in the SC passes through a shallow maximum and goes to zero following a strict T^2-dependence (see inset of figure 5). In canonical spin glasses also a cusp-shaped maximum is observed slightly above the freezing temperature, but a linear term evolves towards zero temperature [4]. Regarding the magnetization measurements in $FeCr_2S_4$, a spin-glass state is very unlikely [23]. Thus, the absence of the λ-type anomaly and the shallow maximum observed in the $FeCr_2S_4$ SC suggests a glassy-like state of the orbitals. The T^2-dependence of the heat capacity for temperatures below the maximum is theoretically not expected for disordered spin-systems, but has also been observed in the ordered spinel AlV_2O_4 [24] and in two-dimensional

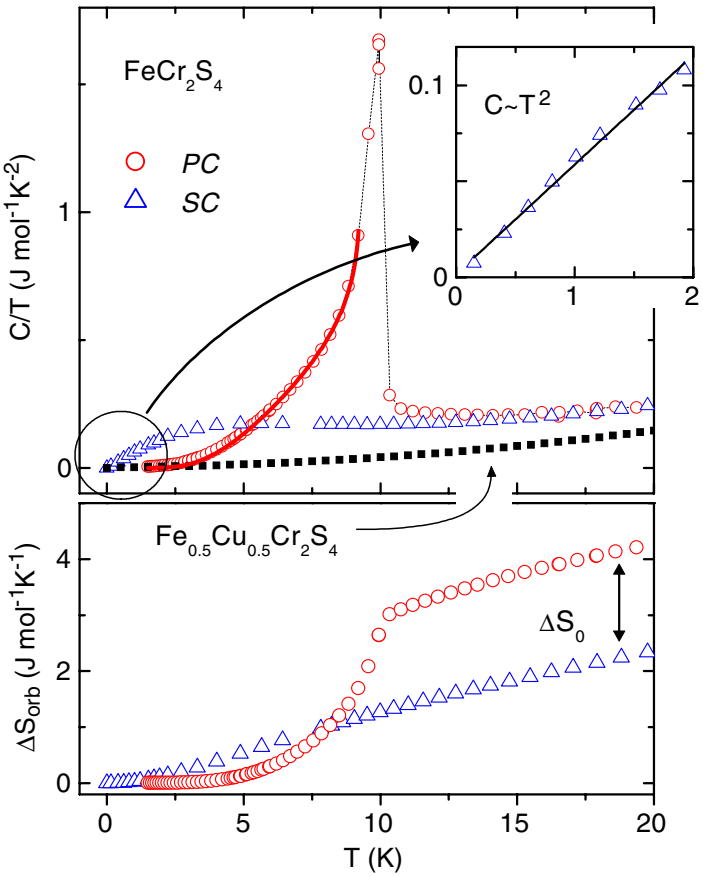

Figure 5. Upper panel: temperature dependence of the heat capacity in the representation $C/T(T)$ versus T of the PC sample and SC. The PC exhibits an anomaly at $T_{OO} = 10$ K. The solid line represents a fit to a mean-field approach (see text). Inset: a magnification of the low-temperature data of the SC. Solid squares: C/T of $Fe_{0.5}Cu_{0.5}Cr_2S_4$ SC, indicating the magnon and the phonon contribution. Lower panel: entropy change ΔS_{orb} versus temperature T for the SC and the PC calculated from the data in the upper panel after subtraction of the magnon and phonon contribution. ΔS_0 indicates the entropy difference between SC and PC samples determined in the orbital-liquid regime ($T > T_{OO}$).

spin glasses [25]. It has been shown by Ivanov *et al* [26] that random fields can suppress orbital order and that in systems, where orbital order is absent, the heat capacity follows the power-law $C \propto T^2$, which we observed experimentally. The origin of the observed orbital glass behaviour may be attributed to the small amount of hole doping by chlorine ions (less than 1%) on sulfur places mentioned above.

Note that above the ordering temperature ($T > T_{OO}$) all samples reveal a very similar heat capacity with a highly enhanced linear term. The comparison with the heat capacity of the related compound $Fe_{0.5}Cu_{0.5}Cr_2S_4$ with similar atomic mass and Debye temperature as $FeCr_2S_4$ demonstrates that the highly enhanced heat capacity can neither be explained by a T^3 phonon nor a $T^{3/2}$ magnon contribution: in $Fe_{0.5}Cu_{0.5}Cr_2S_4$, the Cu ions are monovalent and all Fe ions have a valence of 3+ ($3d^5$, $S = 5/2$) and, hence, are not JT active, because of the

half-occupied 3d shell. It is a simple ferrimagnet, whose heat capacity can be well described by the superposition of a T^3-law for the phonons and a $T^{3/2}$-law for the magnons. As the fitting formula we used $C(T) = (12\pi^4/5)rN_A k_B(T/\Theta_D)^3 + \delta T^{3/2}$, where r is the number of atoms within an unit cell, N_A the Avogadro's constant and k_B the Boltzmann constant. The free fitting parameter Θ_D and δ are the Debye temperature and the magnon contribution, respectively, yielding the values $\Theta_D = 343$ K and $\delta = 2.5\,\mathrm{mJ\,mol^{-1}\,K^{-5/2}}$. These values are very reasonable regarding the literature data of magnetite Fe_3O_4 given as $\Theta_D = 660$ K and $\delta = 1.315\,\mathrm{mJ\,mol^{-1}\,K^{-5/2}}$ [27]. The smaller Debye temperature Θ_D in $Fe_{0.5}Cu_{0.5}Cr_2S_4$ can be explained by the higher molar mass and the weaker bond strength due to the larger sulfur lattice as compared to the oxygen lattice in magnetite. The magnon contribution [27] scales with the exchange constant $\delta \propto J^{-3/2}$ which itself is higher in magnetite ($T_C = 848$ K) than in $Fe_{0.5}Cu_{0.5}Cr_2S_4$ ($T_C = 275$ K). This explains the higher δ value in $Fe_{0.5}Cu_{0.5}Cr_2S_4$ in comparison with Fe_3O_4.

Subtraction of these estimated phonon and magnon contributions from the low-temperature heat capacity of $FeCr_2S_4$ reveals an additional linear contribution to the heat capacity C of the order of $\Delta C/T \approx 100\,\mathrm{mJ\,mol^{-1}\,K^{-2}}$ in this compound visible as an offset in the $C(T)/T$ representation at elevated temperatures $T > 10$ K (upper frame of figure 5). This contribution cannot be attributed to an enhanced Sommerfeld coefficient because $FeCr_2S_4$ is insulating at low temperatures [28, 29]. Therefore, we ascribe it to the strongly fluctuating orbitals. It is worth to note that a linear term in the temperature dependence of the heat capacity has been already predicted for the orbital liquid [13]. Furthermore, the existence of a dynamic JT effect has been originally deduced from Mössbauer experiments [30] and later on has been termed as orbital paramagnetism regarding its cooperative properties involving the B-site Cr states [31]. The dynamic JT effect as well as orbital paramagnetism indicates orbital fluctuations and in their cooperative manner provide an orbital-liquid state. To summarize the results of the heat capacity in $FeCr_2S_4$, we conclude that for temperatures $T > 10$ K an orbital-liquid state is formed in $FeCr_2S_4$. The gap predicted for orbital liquids in the orbital-excitation spectrum [32] must be very small, as in the SC the linear term persists down to approximately 3 K and no exponential decay is observed to lower temperatures. In the PC, a transition occurs from the orbital-liquid into the orbitally ordered state at 10 K. In the SC, the OO transition is suppressed and, taking into account the shallow maximum and decrease of the heat capacity at lowest temperatures, we suggest that the orbital degrees of freedom undergo a freezing transition into an orbital-glass state with randomly frozen-in orbital configurations.

In order to corroborate these findings, we calculated the entropy in $FeCr_2S_4$ which is shown in the lower frame of figure 5. The entropy $\Delta S_{orb}(T)$ has been obtained by integrating $C(T)/T$ for temperatures $0.1 < T < 20$ K. The excess heat capacity ΔC has been determined by subtracting the estimated phonon and magnon contributions as described above. In the orbitally ordered PC, the entropy goes to zero below the JT transition. Above T_{OO} the entropy is further increasing indicating that not the full entropy $R \ln 2 = 5.8\,\mathrm{J\,mol^{-1}\,K^{-1}}$ of the orbital doublet has been recovered in agreement with the observation of an orbital liquid. The entropy of the frustrated system has a lack of entropy of approximately $\Delta S_0 \approx 2\,\mathrm{J\,mol^{-1}\,K^{-1}}$ at 10 K (see lower frame of figure 5). This shortfall of 1/3 of the total orbital entropy surprisingly coincides approximately with the result in the spin-ice system [6].

The heat capacity of $MnSc_2S_4$ and $FeSc_2S_4$ is documented in figure 6 for temperatures $1.5 < T < 50$ K. In addition, the phonon contribution is plotted which was estimated by measuring the non-magnetic spinel $CdIn_2S_4$ (for details see [17]). In all samples the lattice-derived heat capacity dominates above 20 K. However, it is impressive to see, how in the geometrically

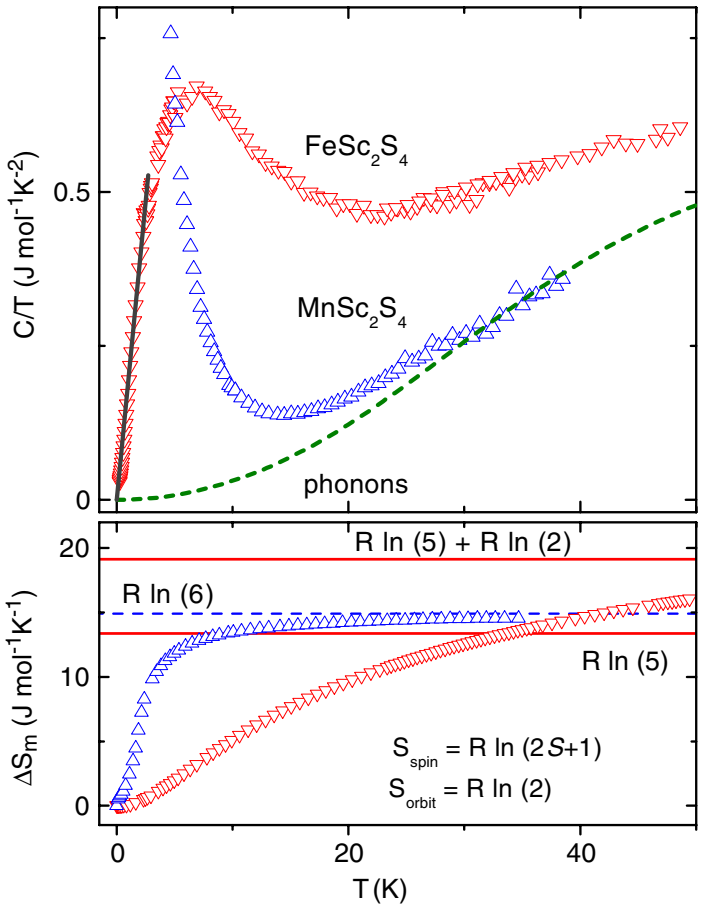

Figure 6. Upper panel: heat capacity $C(T)/T$ versus T of $FeSc_2S_4$ (triangles down) and $MnSc_2S_4$ (triangles up). The dashed line gives the estimated phonon contribution (for details see [17]). The solid line indicates the behaviour $C(T) \propto T^2$. Lower panel: magnetic entropy $\Delta S_m(T)$ of $FeSc_2S_4$ and $MnSc_2S_4$. The horizontal lines give the magnetic entropy S_m, which is theoretically expected for the spin and orbital degrees of freedom (see text).

frustrated systems the heat capacity is enhanced towards low temperatures, having in mind that the characteristic magnetic temperatures are 23 and 45 K as determined via the CW susceptibilities for the Mn and Fe compound, respectively (see sections 2.2 and 2.4). For $MnSc_2S_4$, $C(T)/T$ diverges towards the phase-transition temperature into long-range magnetic order at $T_N \approx 2$ K. $FeSc_2S_4$ reveals a broad peak close to 6 K which often is observed in geometrically frustrated magnets [5]. On further decreasing the temperature, $C(T)/T$ decreases and no indications of an ordering transition were observed for temperatures down to 50 mK [17]. As indicated in the upper frame of figure 6, the low-temperature heat capacity of $FeSc_2S_4$ can be approximated by a T^2 behaviour, similar to the experimental findings in $FeCr_2S_4$ (see inset in the upper frame of figure 5). This temperature dependence again provides some experimental evidence for the existence of an orbital-glass state in $FeSc_2S_4$, too. Thus, this material reveals a spin-liquid and orbital-glass state at low temperatures.

Subtracting the phonon contribution, we again calculated the magnetic entropy ΔS_m as described above. The entropy $\Delta S_m(T)$ is plotted in the lower frame of figure 6. We found that for

$MnSc_2S_4$ only 80% of the expected entropy for a spin $S = 5/2$ system are recovered at $T = 10$ K corresponding to five times the ordering temperature $T_N \approx 2$ K. The full entropy is reached at a temperature $T \approx -\Theta_{CW}$. For $FeSc_2S_4$, the entropy slowly increases with increasing temperature reaching $S_m = R\ln(5)$ J mol^{-1} K^{-1} corresponding to an $S = 2$ system at $T \approx 30$ K. It shows a significant further increase towards a value of $\Delta S_m = (R\ln(5) + R\ln(2))$ J mol^{-1} K^{-1}, where the latter term characterizes the entropy of the orbital doublet of the JT active e levels. From the magnetic entropy ΔS_m in the lower frame of figure 6, we attribute $MnSc_2S_4$ to a spin liquid for temperatures $2 < T < 23$ K whereas in the case of $FeSc_2S_4$ an additional contribution to the magnetic entropy comes presumably from the frustrated orbital state. Therefore, $FeSc_2S_4$ can be considered as a spin–orbit liquid for temperatures below 45 K.

2.4. NMR

The NMR measurements were carried out with a phase-coherent pulse spectrometer using field sweeps at constant radio frequencies $\omega_0/2\pi$ =10, 35 and 90 MHz. The spectra were collected by conventional 10 μs–τ_D–20 μs spin-echo pulse sequences with a delay time $\tau_D = 40$ μs between the pulses. NMR provides a highly local probe of electronic moments on an atomic scale. Due to hyperfine interactions of the resonant nuclei with spin and orbital degrees of freedom, the paramagnetic lineshift K of the NMR line monitors the local susceptibility of electron magnetic moments via the relation $K = A_{hf}\chi$ with the hyperfine coupling constant A_{hf}. In addition, the resonant nuclei possessing an electric quadrupole moment are also sensitive to the surrounding charge distribution. This charge distribution either stems from the ligand-field of ionic charges or from the shape of the electron cloud at the nuclear site which is represented by the electronic orbitals. In both cases, the interaction of the nuclear quadrupole moment with the electrical field gradient (EFG) of the surrounding charge distribution can yield a broadening or splitting of the NMR spectra in central and satellite lines. The latter case of an onsite EFG has already been investigated by ^{57}Fe Mössbauer spectroscopy at the A-site in $FeSc_2S_4$ and a drastic increase of the EFG with decreasing temperature was observed [33]. This behaviour was explained by random strains lifting the degeneracy of the orbital states of the e doublet in addition to the conventional crystal-field splitting.

In figure 7(a), we show spectra of the ^{45}Sc nuclei residing on the octahedral B-site in $FeSc_2S_4$ at an irradiation frequency of $\omega_0/2\pi = 10$ MHz. The powder pattern exhibits strongly broadened Gaussian lines without any indications of a splitting in central and satellite lines. Due to the trigonal distortion of the B-sites, the ^{45}Sc spectra are expected to be broadened by quadrupole interaction between the nuclear quadrupole moment of the ^{45}Sc nuclei and the EFG of the distorted sulfur octahedron [38]. Indeed, calculating the broadening contribution due to dipolar interactions between ^{45}Sc nuclear moments corresponding to the Van Vleck formula [34] yields $\Delta H_{dipolar} \approx 2.8$ kHz, which turns out to be negligible compared to the observed linewidth ΔH documented in figure 7(b). Therefore, the broadening of the powder pattern appears to be dominated by quadrupole interaction, where the linewidth ΔH is proportional to the EFG at the B-site. The drastic increase of $\Delta H(T)$ indicated by power-law behaviour in figure 7(b) towards lower temperatures resembles the temperature dependence of the EFG at the A-site deduced from Mössbauer results [33].

In figure 8, the temperature dependence of the inverse local susceptibility represented by $1/K(T)$ is plotted at irradiation frequencies of $\omega_0/2\pi = 10$, 35 and 90 MHz.These irradiation frequencies correspond to applied magnetic fields of 9.5, 33 and 87 kOe, respectively.

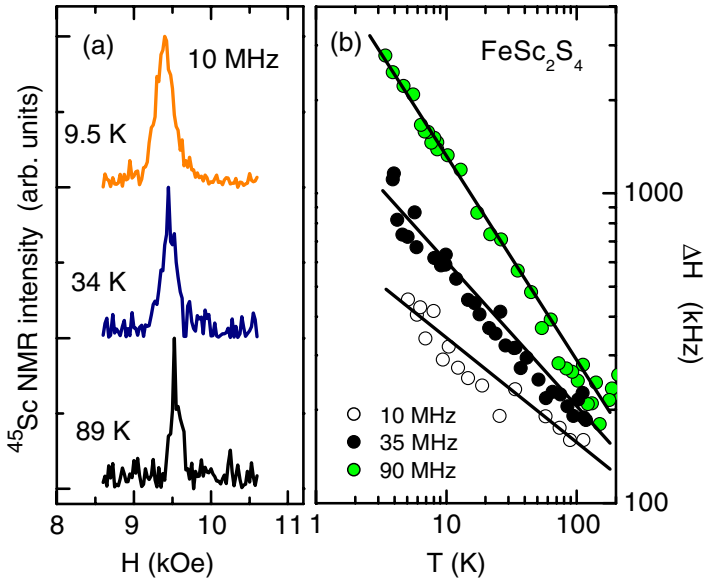

Figure 7. (a) ^{45}Sc NMR spectra of $FeSc_2S_4$ at 10 MHz and different temperatures. (b) Temperature dependence of the NMR linewidth $\Delta H(T)$ (full width at half maximum). Solid lines indicate a power-law behaviour for 10 MHz (9.5 kOe), 35 MHz (33 kOe) and 90 MHz (87 kOe), respectively.

Extrapolating the high-temperature data towards the intersection with the temperature axis, we obtain the CW temperature $\Theta_{CW} = -45$ K of $FeSc_2S_4$ as it is indicated by the solid line in figure 8. For temperatures $T < 40$ K, a significant deviation from the CW law occurs and the local susceptibility $K(T)$ becomes temperature independent for the lowest temperatures (see the inset of figure 8). This leveling-off reminds one of low-dimensional antiferromagnetically correlated systems, where the susceptibility $\chi(T)$ exhibits a characteristic maximum. But in addition, this behaviour of $K(T)$ turned out to be also characteristic for a number of prominent triangular frustrated spin systems $LiNiO_2$ [35], $SrCr_8Ga_4O_{19}$ [36] and $Ba_2Sn_2ZnCr_{7p}Ga_{10-7p}O_{22}$ [37] and, hence, underlines the strong magnetic frustration of $FeSc_2S_4$ in the spin sector.

2.5. Neutron scattering

To elucidate the nature of the spin and orbital quantum liquid it is essential to study the electronic excitation spectrum. We are not aware of any spectroscopic evidence of an orbital-liquid state. But there exists a number of neutron-scattering experiments on geometrically frustrated spin systems: spin fluctuations with a characteristic energy width and a weak temperature dependence have been observed in metallic and frustrated $Y : ScMn_2$ and in geometrically frustrated β-Mn [39]. Later on, the ground state of this latter compound has been characterized as non-Fermi liquid [40]. Competing ferromagnetic and antiferromagnetic spin fluctuations occur in the quasi-elastic excitation spectrum of the frustrated heavy-fermion system LiV_2O_4 [41]–[43]. Turning to insulating frustrated magnets, for $ZnCr_2O_4$, with the Cr spins residing on a pyrochlore lattice, Lee *et al* [44] demonstrated that groups of six spins form weakly interacting antiferromagnetic loops. There also exist a number of neutron-scattering studies of the magnetic excitation spectra in frustrated organometallic magnets [45, 46].

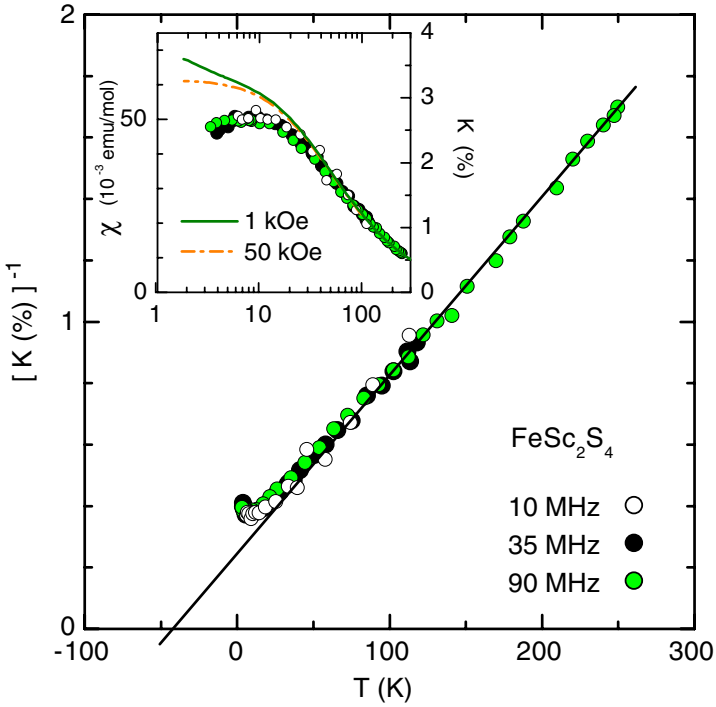

Figure 8. ^{45}Sc NMR: inverse lineshift $1/K(T)$ of $FeSc_2S_4$ at 10 MHz (9.5 kOe), 35 MHz (33 kOe) and 90 MHz (87 kOe), respectively. The solid line extrapolates a CW law $\chi = C/(T - \Theta_{CW})$ with $\Theta_{CW} = -45$ K. Inset: bulk susceptibility $\chi(T)$ (solid and dashed lines) and lineshift $K(T)$ (symbols) as the local susceptibility.

The inelastic neutron scattering experiments have been performed on the time-of-flight spectrometers IN4 and IN6 at the Institute Laue Langevin (ILL), Grenoble. The spectrometer IN6 employing cold neutrons is particularly well suited for high-resolution measurements in the low-Q/low-energy transfer region, whereas IN4 located at a thermal beam tube allows to access an extended Q/energy-range (up to 12 meV energy transfer and 5.4 Å^{-1} in the present case). Carefully powdered samples were filled in a flat-plate aluminum sample holder and mounted in a cryostat allowing for temperatures $1.5 \leqslant T \leqslant 300$ K. Additionally, a vanadium standard and an empty sample holder were measured to account for detector efficiency and background signal, respectively. The raw data were corrected in a standard way employing the LAMP program package of the ILL. The measured dynamic structure factor is directly proportional to the imaginary part of the generalized susceptibility via $S(Q, \omega) = [1 - \exp(-\hbar\omega/k_B T)]^{-1} \chi''(Q, \omega)$. Apart from resolution-limited incoherent scattering contributions around zero energy transfer, the data obtained on IN4 show additional magnetic intensities which extend up to energies of approximately 5 meV corresponding to the magnitude of the magnetic exchange in the system. At low temperatures $T = 1.6$ K, these intensities reveal a significant modulation in Q thus pointing towards antiferromagnetic exchange. In addition, a roughly Q-independent inelastic signal is observed around 2 meV energy transfer for all measured temperatures, even at 80 K. This is documented in the upper frame of figure 9, where a cut at $Q = 1.1$ Å^{-1} for 1.6 K and 80 K is plotted and a clear inelastic contribution

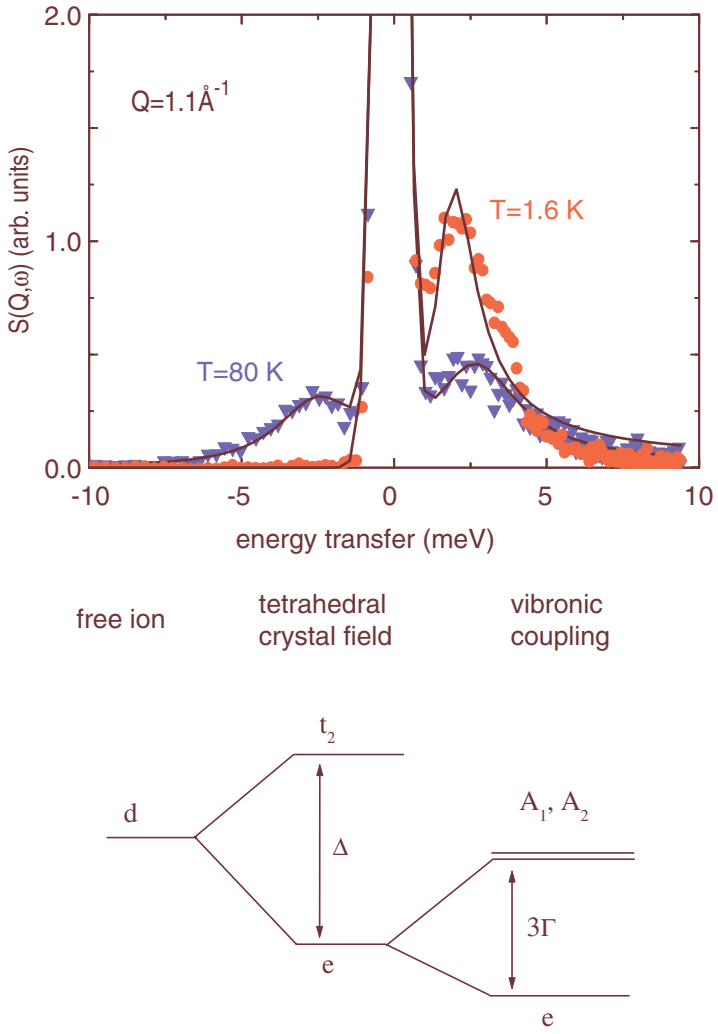

Figure 9. Upper panel: dynamical structure factor $S(Q, \omega)$ of $FeSc_2S_4$ at constant $Q = 1.1$ Å^{-1} at $T = 80$ K (blue triangles) and at $T = 1.6$ K (red circles). The full black line is a fit to the data employing a single inelastic Lorentzian line, multiplied by the detailed balance factor and convoluted with the instrumental resolution. Lower panel: the dynamic JT effect is illustrated by the vibronic splitting of the electronic configuration in addition to the conventional crystal-field splitting.

with excitation energies of approximately 2 meV is present. With decreasing temperature the excitation energies $\hbar\omega$ soften and the damping γ decreases ($T = 80$ K: $\hbar\omega = 2.4$ meV, $\gamma = 1.6$ meV; $T = 1.5$ K: $\hbar\omega = 1.73$ meV, $\gamma = 0.80$ meV). We interpret this excitation as a possible signature of the orbital-liquid state, a hypothesis which is substantiated as follows. The electronic ground state of tetrahedrally coordinated Fe^{2+} is a hole in the e doublet, which is JT active. It is well known that the JT effect may be either static or dynamic. The static JT effect results from a strong coupling between the electronic and the lattice degrees of freedom, giving rise to a long-range ordered lattice distortion. But if the coupling is weak, no static distortion appears. Instead, a coupled motion of electronic and vibrational modes results, which is referred

to as dynamic JT effect and is described for the single-ion case in detail by Ham [47]. In this case, the electronic ground state remains an e state, separated by 3Γ from the first excited vibronic levels A_1 and A_2. This situation is depicted in the lower frame of figure 9 which shows the crystal-field splitting and the additional vibronic splitting due to a weak JT effect. In the case of $FeSc_2S_4$, the dynamic JT effect yielding a vibronic splitting of the coupled electronic and vibrational modes characterizes the orbital liquid. A similar model, including additional strain effects has been utilized to explain the early Mössbauer experiments on $FeSc_2S_4$ [33]. In these experiments, the dynamic JT effect has been detected well above 100 K. But it has to be clearly stated that other explanations cannot be discarded completely, e.g. this unusual excitation could also result from a moderate spin–orbit coupling, splitting the ground-state doublet.

Measurements on the high-resolution time-of-flight spectrometer IN6 provide more detailed information in the low-Q and low energy-transfer region. Again, strong incoherent intensities caused by elastic processes show up close to zero-energy transfer with a clear signature of the first three nuclear Bragg reflections. We note that even at 1.6 K neither indications of magnetic Bragg reflections nor indications of a splitting of the nuclear Bragg reflections due to a structural transition become apparent. And indeed heat capacity measurements demonstrated the absence of a structural, as well as of a magnetic phase transition down to 50 mK [17]. Already at 80 K, in addition to the elastic contributions, inelastic magnetic intensities show up, which are centred around $Q = 0.6$ and $1.44\,\text{Å}^{-1}$, respectively. These values of momentum transfer correspond to the expected magnetic Bragg-peak positions (Brillouin-zone centre) for antiferromagnetic ordering and thus indicate that strong antiferromagnetic spin fluctuations are present already far above the virtual ordering temperature of $-\Theta_{CW} \approx 45$ K, estimated from the CW law of the susceptibility (see sections 2.2 and 2.4). Spin fluctuations are commonly observed in the paramagnetic phase of frustrated magnets. However, on cooling drastic changes appear in the magnetic excitation spectrum despite the fact that $FeSc_2S_4$ is still paramagnetic. The inelastic magnetic intensities become softer around $Q = 0.6$ and $1.44\,\text{Å}^{-1}$ and develop a spin-wave like dispersion. This is illustrated in figure 10 showing the magnetic excitation spectra at $T = 1.6$ K for three different constant energy transfers. In the lowest frame of figure 10, for low-energy transfers $\hbar\omega = 0.2$ meV, the tails of three nuclear Bragg peaks are present, which are indexed accordingly. Furthermore, magnetic intensities are centred around $Q = 0.6$ and $1.44\,\text{Å}^{-1}$ and can be fitted by a single Lorentzian line. For increasing energy transfers however (middle and upper frames of figure 10), the magnetic intensities shift their position and a clear double-peak structure can be resolved. Starting from the elastic positions expected for antiferromagnetic ordering the corresponding magnetic intensities separate in a manner resembling that of a spin-wave dispersion branch. However, there are no indications of long-range magnetic order. These intensities indicate significant scattering of magnetic excitations and remind one of a spectrum of a paramagnet just above the antiferromagnetic ordering temperature. Our present inelastic neutron-scattering results on $FeSc_2S_4$ reveal a cross-over from a system with strong antiferromagnetic spin fluctuations at $T > -\Theta_{CW}$ to a really cooperative paramagnet with fully isotropic magnon-like excitations at low temperatures ($T \leqslant -\Theta_{CW}$).

2.6. Dielectric spectroscopy

For the dielectric measurements, silver paint contacts were applied to the plate-like samples forming a parallel-plate capacitor. The conductivity and permittivity were measured over a

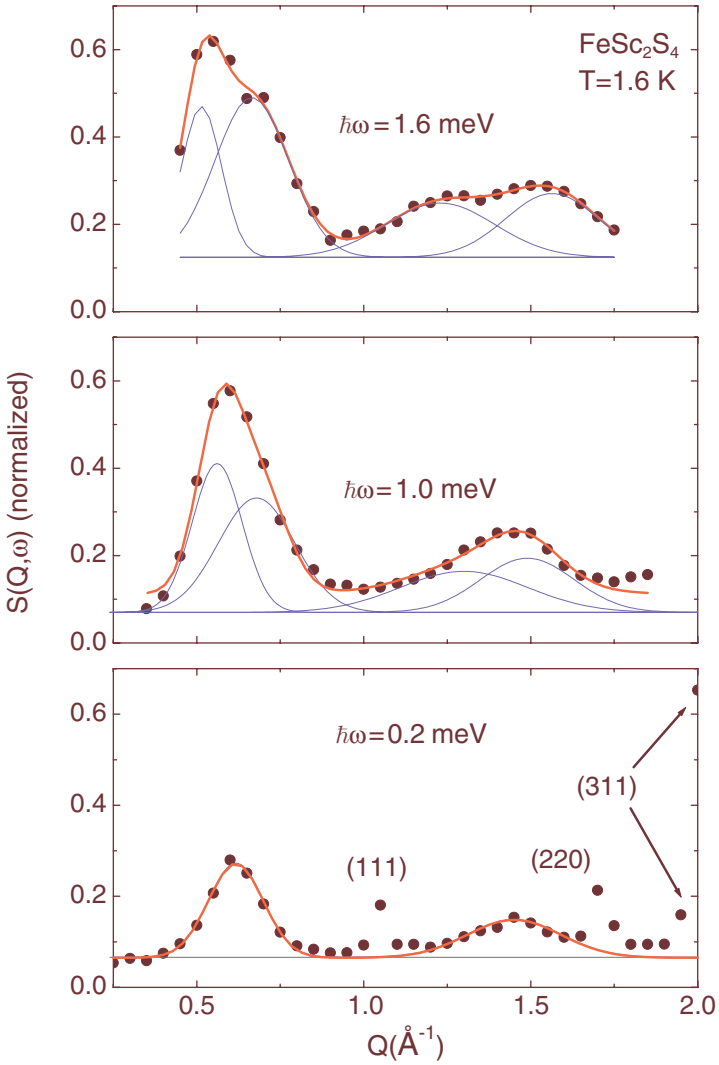

Figure 10. Magnetic excitation spectra of $FeSc_2S_4$ at $T = 1.6\,K$ for three different constant energy transfers. In the lowest panel at $\hbar\omega = 0.2\,meV$ some tails of the nuclear Bragg reflections can be still seen and are indexed accordingly. Upon higher energy transfers, the magnetic intensities starting at the expected magnetic Bragg-peak positions (Brillouin zone centre) separate in a spin-wave dispersion-like manner.

broad frequency range of nine decades ($0.1\,Hz < \nu < 100\,MHz$) at temperatures down to 1.4 K. A frequency-response analyser (Novocontrol α-analyser) was used for frequencies $\nu < 1$ MHz and a reflectometric technique employing an impedance analyser (Agilent E 4291A) at $\nu > 1$ MHz [48].

Dielectric spectroscopy is a well-established technique for the investigation of the molecular dynamics in liquids and supercooled liquids, giving valuable information concerning the relaxational behaviour and the many-decades change of time scales during glassy freezing (see, e.g., [49, 50]). Thus, it is useful to employ dielectric spectroscopy also for the investigation of the liquid- or even glass-like orbital dynamics, suggested for $FeCr_2S_4$ and $FeSc_2S_4$ to arise

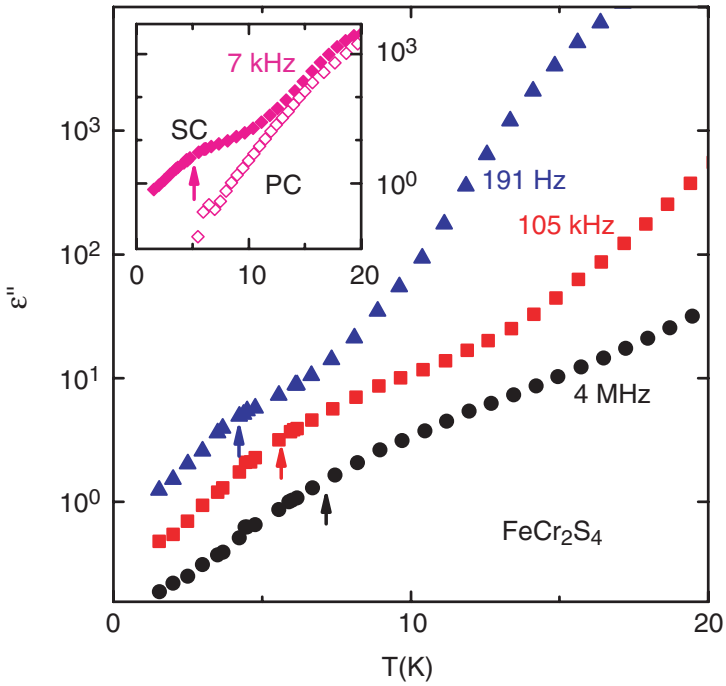

Figure 11. Temperature dependence of the dielectric loss in SC $FeCr_2S_4$ for selected frequencies. The arrows indicate the position of the underlying relaxation loss peaks. Inset: comparison of the dielectric loss in SC and PC material at 7 kHz.

from geometrical frustration effects (see sections 2.2 and 2.3). Of course, a prerequisite for the applicability of this technique is the coupling of the electrical field to the orbital degrees of freedom. In JT-active systems as $FeCr_2S_4$ and $FeSc_2S_4$, such a coupling may arise from the fact that the orbital reorientations are coupled to the elastic response of the ionic lattice via electron–phonon interactions and, thus, any orbital reorientation is accompanied by a redistribution of charges. Here, we provide the results of a dielectric investigation of the orbital dynamics in $FeCr_2S_4$ and $FeSc_2S_4$, indeed showing a distinct relaxation-like behaviour, which can be ascribed to the freezing of orbital degrees of freedom. The mean relaxation time is derived, revealing glass-like slowing down, however, the actual glass-transition being suppressed by quantum-mechanical fluctuations.

Figure 11 shows the dielectric loss ε'' of SC $FeCr_2S_4$ for various frequencies at temperatures below 20 K. Above about 10 K, the behaviour is dominated by charge transport, leading to a strong increase with temperature (for details see [51]). However, as indicated by the arrows, superimposed to this contribution, there is a significant shoulder, indicating an underlying peak that shifts towards lower temperatures with decreasing frequency. This is the typical signature of relaxational behaviour as commonly observed, e.g., for the glassy freezing of dipolar molecules in supercooled liquids or orientational glasses [49, 50, 52]. The loss peak arises when the temperature-dependent relaxation time equals the inverse angular frequency, leading to maximum absorption of power from the field. This relaxational feature occurs in just the same temperature region, where evidence for glassy freezing of the orbital dynamics was deduced from heat-capacity measurements revealing a shallow cusp in C/T versus T at about 5 K (see the upper frame of figure 5). Thus, the detected dielectric relaxation can be assumed to mirror the glass-like

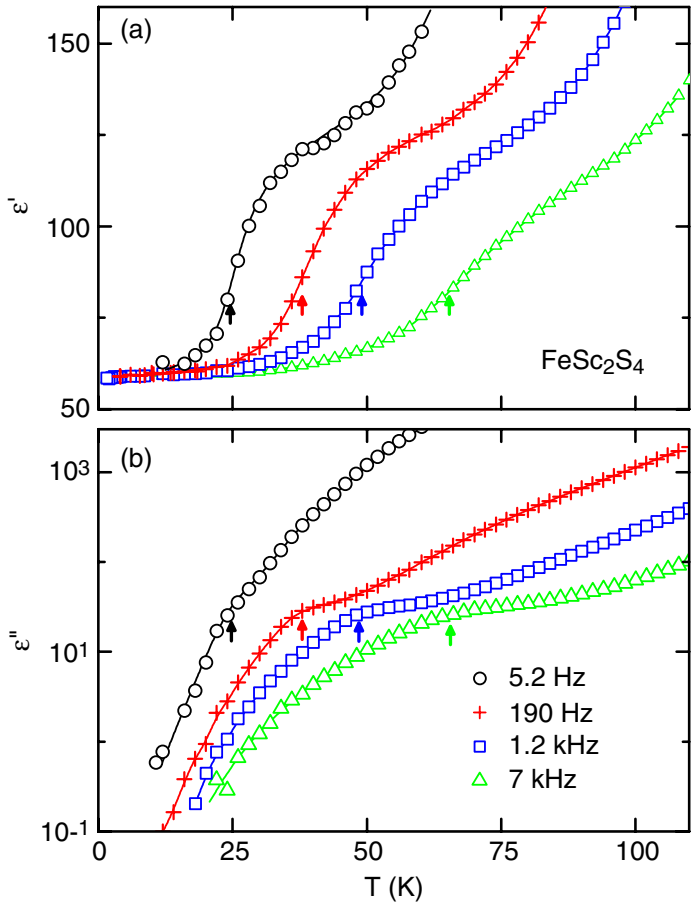

Figure 12. Temperature dependence of the dielectric constant (a) and loss (b) in SC $FeSc_2S_4$ for selected frequencies. The arrows indicate the position of the relaxational feature.

slowing down of orbital dynamics. Further evidence for this notion arises from a comparison to the results on a PC sample (inset of figure 11), where the orbital degrees of freedom were found to be ordered at low temperatures (for more details see [18, 51]). While the conductivity background is nearly identical, the relaxation feature is completely missing in the PC, ε'' being more than one decade smaller at the peak temperature of the corresponding SC curve. This finding strongly corroborates the view of orbital reorientations leading to the observed relaxation feature.

In figure 12, the temperature dependence of the dielectric constant and loss, measured on SC $FeSc_2S_4$ at selected frequencies are plotted. In this material, being isostructural to $FeCr_2S_4$, a clear signature of relaxational behaviour shows up, too. Well-developed shoulders in $\varepsilon''(T)$, indicating an underlying loss peak as in $FeCr_2S_4$ (see figure 11), are accompanied by a step-like decrease towards low frequencies in $\varepsilon'(T)$, characteristic for glass-like freezing. When cooling, the orbital reorientations become effectively stuck compared to the time scale given by the exiting ac-field, thus, leading to the observed step-like reduction of $\varepsilon'(T)$. Hence, we conclude that in $FeSc_2S_4$ also the orbital dynamics shows a glass-like slowing down towards low temperatures. This again agrees with the finding of a broad peak in the low-temperature heat capacity of this material [17], characteristic for glassy freezing [53] (section 2.3). In addition, in [33], just in

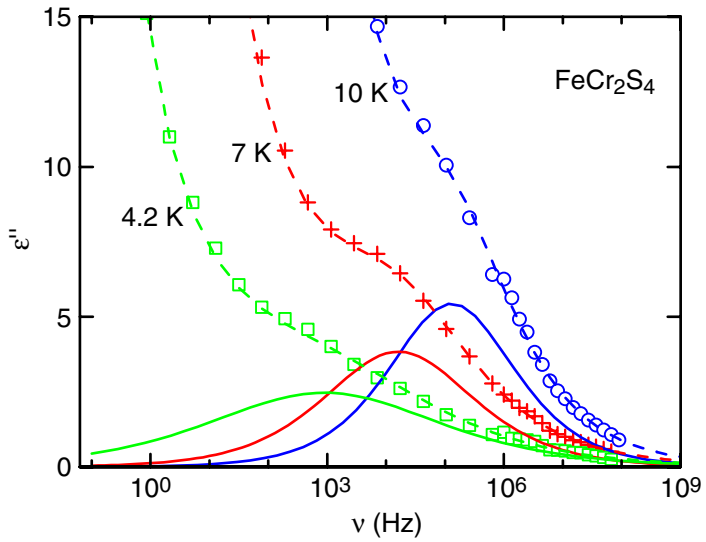

Figure 13. Dielectric loss versus frequency at three temperatures $T \leqslant 10$ K. The dashed lines represent the results of fits as described in the text. The solid lines characterize the contributions due to the orbital relaxations.

the temperature region, where we observe glassy dynamics in our experiments, a broadening of Mössbauer lines was observed for $FeSc_2S_4$, which can be taken as indication of a slowed-down orbital motion.

To obtain information on the relaxation time and other parameters characterizing the orbital relaxation, it is advantageous to analyse the frequency-dependent data [49, 50, 52]. Figure 13 shows $\varepsilon''(\nu)$ of $FeCr_2S_4$ for selected temperatures. The frequency-dependent loss tends to diverge towards low frequencies, which, as ε'' is proportional to σ'/ν, can be ascribed to a strong conductivity contribution. Superimposed to this behaviour, a shoulder indicating an underlying loss peak is observed, which corresponds to the shoulder observed in the temperature dependence (see figure 11). As the peak frequency is inversely proportional to the relaxation time, its continuous shift towards lower frequencies with decreasing temperature directly mirrors the glass-like slowing down of the orbital dynamics, when cooling below 10 K. The dashed lines in figure 13 are fits with the sum of the phenomenological Cole–Cole (CC) function [50, 54], often employed to parametrize loss peaks in canonical and orientational glasses, and a conductivity contribution (for details see [51]). Good agreement of fits and experimental spectra could be achieved in this way, the solid lines showing the relaxational part of the fits. Very broad loss peaks are revealed, their widths strongly increasing towards low temperatures. For the renowned Debye case, where an identical exponential time-dependence for all relaxing entities is assumed, loss peaks with a half-width of 1.14 decades are expected [50]. This is clearly exceeded in the present case. Thus, the relaxation in $FeCr_2S_4$ shows the typical broadening, characteristic for glassy systems, which is commonly ascribed to a disorder-induced heterogeneous distribution of relaxation times [50, 53]. With decreasing temperature the peak width increases significantly, while its amplitude decreases. Such a behaviour is usually observed in the so-called orientational glasses, crystalline materials where the molecules exhibit frustration-induced disorder with respect to the orientational degrees of freedom [52]. It can be explained assuming a temperature-independent Gaussian distribution of energy barriers hindering the reorientational motion [55].

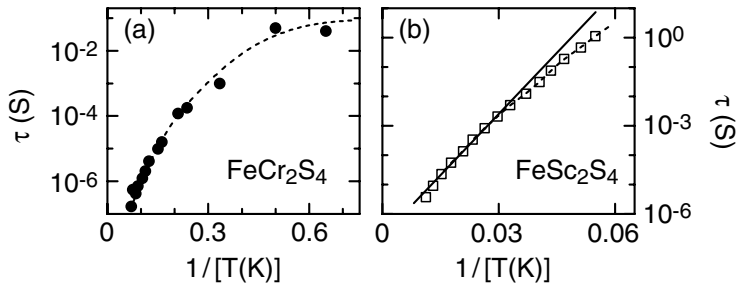

Figure 14. Temperature dependence of the relaxation time of $FeCr_2S_4$ (a) and $FeSc_2S_4$ (b). The dashed lines are guides to the eye. The solid line in (b) indicates thermally activated behaviour with an energy barrier of 27 meV.

The most significant parameter characterizing glassy freezing is the temperature development of the relaxation time. As revealed in figure 14, for both materials investigated, the relaxation time τ characterizing the reorientational dynamics of the orbitals shows a smooth slowing down over an extremely broad range (up to six decades) with decreasing temperature, which is typical for glassy freezing. In the Arrhenius representation of figure 14, a purely thermally activated process corresponds to a straight line. At the higher temperatures, the curves in figure 14 may be approximated by such a behaviour as is indicated for $FeSc_2S_4$ by the solid line corresponding to an energy barrier of 27 meV. However, in contrast to most other glassy systems, the temperature dependence of τ becomes weaker for low temperatures, for $FeCr_2S_4$ even seeming to level off at a constant value of about 0.1 s (see figure 14(a)). A constant $\tau(T)$ can be explained by tunnelling processes driving the orbital reorientations and, hence, we interpret the overall behaviour as a smooth transition from a thermally activated to tunnelling-dominated dynamics towards low temperatures. As already evident from a comparison of figures 11 and 12, the temperature range of the glassy slowing down of orbital motion in $FeSc_2S_4$ is higher than in $FeCr_2S_4$. Thus, thermally activated behaviour dominates in this material, tunnelling processes leading to small deviations below about 30 K only (see figure 14(b)). It should be noted that, especially for $FeCr_2S_4$, the onset of tunnelling may prevent the relaxation time to become larger than 100 s, a limit where for canonical glass formers the glass transition is defined [53]. Therefore, strictly speaking, within this conventional definition of the glass transition the actual orbital-glass state may not be realized in these materials. But of course, relaxation rates in the sub-Hz region as detected here certainly are extremely slow for electronic degrees of freedom.

Concluding this section, by dielectric spectroscopy at low temperatures we achieved a thorough characterization of the glassy freezing of the orbital degrees of freedom in $FeCr_2S_4$ and $FeSc_2S_4$. We find typical glassy behaviour, in particular, a continuous slowing down of the orbital dynamics and a distribution of relaxation times. A complete freezing-in is suppressed by quantum-mechanical tunnelling, limiting the low-temperature relaxation time in $FeCr_2S_4$ to about $\tau \simeq 10^{-1}$ s.

3. Conclusion

In this brief review we reported results on three different sulfur spinels, AB_2S_4, crystallizing in the normal cubic spinel structure. We focus on geometrical frustration effects of orbital moments,

which are located on the A-site of the spinel structure, i.e., Fe^{2+} ions in a tetrahedral environment, which is weakly JT active. $FeCr_2S_4$ is a ferrimagnet below 167 K with a fully developed long-range magnetic order. In this system an orbital liquid is observed, which in PCs undergoes a phase transition into an orbitally ordered state accompanied by an elastic JT distortion, while in SCs the OL state transforms into an orbital glass via a freezing of the orbital moments into a state devoid of long-range order. The orbital glass transition is also evidenced by a shallow cusp in the temperature dependence of the heat capacity followed by a T^2 dependence towards low temperature. The latter has been predicted theoretically for the heat capacity in JT glasses [26]. Despite the discussed influence of the sulfur stoichiometry on the ground state, the quite low temperature of the onset of the cooperative JT effect underlines the vital role of geometric frustration in this system.

That geometrical frustration plays an important role concerning the orbital freezing is strongly supported by similar results observed for $FeSc_2S_4$, a spinel where only the A-site is occupied by Fe^{2+}, having spin and orbital degrees of freedom. In this case, however, the magnetic moments are strongly frustrated and $FeSc_2S_4$ remains paramagnetic down to the lowest temperatures. It is interesting to note that $FeSc_2S_4$ belongs to the class of geometrically frustrated magnets with one of the largest frustration parameters ever observed. Also, in this supercooled paramagnet, the orbital moments freeze into a low-temperature orbital glass, again evidenced by the low-temperature T^2 dependence of the heat capacity. The dynamics of the orbital freezing is directly probed by dielectric spectroscopy, which reveals the slowing down of the orbital degrees of freedom. In both compounds, the thermally activated relaxational reorientations become dominated by quantum-mechanical tunnelling at low temperatures. Strictly speaking, the glass transition becomes suppressed by quantum effects. For $FeSc_2S_4$, the orbital-glass transition is also studied using ^{45}Sc NMR experiments and quasi-elastic neutron-scattering results. The orbital excitations show up via a dynamic JT effect with a splitting of the order of 20 K. The spin liquid is evidenced by the occurrence of magnon-like excitations in the supercooled paramagnet. The results in $FeSc_2S_4$ are contrasted with results on $MnSc_2S_4$, which reveal a half-filled shell and no spin–orbit coupling. In this compound a moderate geometrical frustration is observed in the spin sector.

Acknowledgments

We thank Dr E-W Scheidt for his measurements of the heat capacity at very low temperatures. We are also grateful to Dr H Mutka and Dr M Koza for their help and advise during the neutron-scattering experiments and data analysis. This work was supported by the BMBF via VDI/EKM, FKZ 13N6917-A and by the Deutsche Forschungsgemeinschaft through the Sonderforschungsbereich 484 (Augsburg).

References

[1] Tokura Y and Nagaosa N 2000 *Science* **288** 462
[2] Jahn H A and Teller E 1937 *Proc. R. Soc.* A **161** 220
[3] Kugel K I and Khomskii D I 1982 *Sov. Phys.—Usp.* **25** 2312
[4] Binder K and Young A P 1986 *Rev. Mod. Phys.* **58** 801
[5] Ramirez A P 2001 *Handbook of Magnetic Materials* vol 13, ed K H J Buschow (Amsterdam: Elsevier) p 423
[6] Ramirez A P, Hayashi A, Cava R J, Siddharthan R and Shastry B S 1999 *Nature* **399** 333

[7] Bramwell S P and Gringas M J P 2001 *Science* **249** 1495
[8] Canals B and Lacroix C 1998 *Phys. Rev. Lett.* **80** 2933
[9] Feiner L F, Oles A M and Zaanen J 1997 *Phys. Rev. Lett.* **78** 2799
[10] Ishihara S, Yamanaka M and Nagaosa N 1997 *Phys. Rev.* B **56** 686
[11] Khomskii D I and Mostovoy M V 2003 *J. Phys. A: Math. Gen.* **36** 9197
[12] Keimer B, Casa D, Ivanov A, Lynn J W, von Zimmermann M, Hill J P, Gibbs D, Taguchi Y and Tokura Y 2000 *Phys. Rev. Lett.* **85** 3946
[13] Khaliullin G and Maekawa S 2000 *Phys. Rev. Lett.* **85** 3950
[14] Cwik M, Lorenz T, Baier J, Müller R, André G, Bourée F, Lichtenberg F, Freimuth A, Schmitz R, Müller-Hartmann E and Braden M 2003 *Phys. Rev.* B **68** 060401
[15] Hemberger J, Krug von Nidda H-A, Fritsch V, Deisenhofer J, Lobina S, Rudolf T, Lunkenheimer P, Lichtenberg F, Loidl A, Bruns D and Büchner B 2003 *Phys. Rev. Lett.* **91** 066403
[16] Anderson P W 1956 *Phys. Rev.* **102** 1008
[17] Fritsch V, Hemberger J, Büttgen N, Scheidt E-W, Krug von Nidda H-A, Loidl A and Tsurkan V 2004 *Phys. Rev. Lett.* **92** 116401
[18] Tsurkan V, Fritsch V, Hemberger J, Krimmel A, Mücksch M, Büttgen N, Krug von Nidda H-A, Samusi D, Körner S, Scheidt E-W, Honal M, Horn S, Tidecks R and Loidl A 2004 *Preprint* condmat/0407026
[19] Roth W L 1964 *J. Phys. (Paris)* **25** 507
[20] Reil S, Stork H-J and Haeuseler H 2002 *J. Alloys Compounds* **334** 92
[21] Huang Q, Santoro A, Lynn J W, Erwin R W, Borchers J A, Peng J L and Green R L 1997 *Phys. Rev.* B **55** 14987
[22] Goodenough J B 1963 *Magnetism and the Chemical Bond* (New York: Interscience)
[23] Tsurkan V, Hemberger J, Klemm M, Klimm S, Loidl A, Horn S and Tidecks R 2001 *J. Appl. Phys.* **90** 4639
[24] Matsuno K, Katsufuji T, Mori S, Nohara M, Machida A, Moritomo Y, Kato K, Nishibori E, Takata M, Sakata M, Kitazawa K and Takagi H 2003 *Phys. Rev. Lett.* **90** 096404
[25] Ramirez A P, Espinosa G P and Cooper A S 1990 *Phys. Rev. Lett.* **64** 2070
[26] Ivanov M A, Mitrofanov V Y, Falkovskaya L D and Fishman A Y 1983 *J. Magn. Magn. Mater.* **36** 26
[27] Kouvel J S 1956 *Phys. Rev.* **102** 1489
[28] Ramirez A P, Cava R J and Krajewski J 1997 *Nature* **386** 156
[29] Park M S, Kwon S K, Youn S J and Min B I 1999 *Phys. Rev.* B **59** 10018
[30] Spender M R and Morrish A H 1972 *Solid State Commun.* **11** 1417
[31] Brossard L, Dormann J L, Goldstein L, Gibart P and Renaudin P 1979 *Phys. Rev.* B **20** 2933
[32] Khaliullin G 2001 *Phys. Rev.* B **64** 212405
[33] Brossard L, Oudet H and Gibart P 1976 *J. Phys. (Paris) Colloq.* C6 C6-23
[34] Abragam A 1961 *Principles of Nuclear Magnetism* (New York: Oxford University Press)
[35] Itoh M, Yamada Y, Ubukoshi K, Hirakawa K and Yasuoka H 1986 *J. Phys. Soc. Japan* **55** 2125
[36] Mendels P, Keren A, Limot L, Mekata M, Collin G and Horvatic M 2000 *Phys. Rev. Lett.* **85** 3496
[37] Bono D, Mendels P, Collin G and Blanchard N 2004 *Phys. Rev. Lett.* **92** 217202
[38] Berger S B, Budnick J I and Burch T J 1968 *J. Appl. Phys.* **39** 658
[39] Nakamura H, Yoshimoto K, Shiga M, Nishi M and Kakurai K 1997 *J. Phys.: Condens. Matter* **9** 4701
[40] Stewart J R, Rainford B D, Eccleston R S and Cywinski R 2002 *Phys. Rev. Lett.* **89** 186403
[41] Krimmel A, Loidl A, Klemm M, Horn S and Schober H 1999 *Phys. Rev. Lett.* **82** 2919
[42] Lee S-H, Qiu Y, Broholm C, Ueda Y and Rush J J 2001 *Phys. Rev. Lett.* **86** 5554
[43] Murani A P, Krimmel A, Stewart J R, Smith M, Strobel P, Loidl A and Ibarra-Palos A 2004 *J. Phys.: Condens. Matter* **16** S607
[44] Lee S-H, Broholm C, Ratcliff W, Gasparovic G, Huang Q, Kim T H and Cheong S-W 2002 *Nature* **166** 856
[45] Stone M B, Zaliznyak I, Reich D H and Broholm C 2001 *Phys. Rev.* B **64** 144405
[46] Stone M B, Chen Y, Rittner J, Yardimci H, Reich D H, Broholm C, Ferraris D V and Lectka T 2002 *Phys. Rev.* B **65** 064423
[47] Ham F S 1972 *Electron Paramagnetic Resonance* ed S Gschwind (New York: Plenum)

[48] Schneider U, Lunkenheimer P, Pimenov A, Brand R and Loidl A 2001 *Ferroelectrics* **249** 89
[49] Lunkenheimer P, Schneider U, Brand R and Loidl A 2000 *Contemp. Phys.* **41** 15
[50] Kremer F and Schönhals A (ed) 2003 *Broadband Dielectric Spectroscopy* (Berlin: Springer)
[51] Fichtl R, Lunkenheimer P, Hemberger J, Tsurkan V and Loidl A 2004 *Preprint* cond-mat/0404737
[52] Höchli U T, Knorr K and Loidl A 1990 *Adv. Phys.* **39** 405
[53] Angell C A, Ngai K L, McKenna G B, McMillan P F and Martin S W 2000 *J. Appl. Phys.* **88** 3113
Ediger M D, Angell C A and Nagel S R 1996 *J. Phys. Chem.* **100** 13200
[54] Cole K S and Cole R H 1941 *J. Chem. Phys.* **9** 341
[55] Birge N O, Jeong Y H, Nagel S R, Bhattacharya S and Susman S 1984 *Phys. Rev.* B **30** 2306